Contribution of Physical Layer Uncertainties To Directed Energy Applications[©]

Salvatore Alfano[*]
Christopher T. Kucera[†]
David Finkleman[‡]

Abstract

The objective of this paper is to quantify the influences of air and space borne platform related uncertainties upon directed energy applications. It opens a spectrum of approaches to laser employment by quantifying the risk of illuminating aircraft or satellites unintentionally. .

The formalism of modern communications applies to lasers transmitted over long distances. It is communications with a punch. The Open Systems Interconnect (OSI) formalism decomposes information and energy transfer into seven to nine " protocol layers." The physical layer encompasses characteristics of the propagation environment. It is analogous to the topography of a region. The link layer enables access to the medium, similar to mapping road networks. The network layer establishes routes between transmitter and receiver, determining the address of the recipient and following specific roads to get there. The transport layer accomplishes delivery of information or energy that meets criteria. In communication networks, Transfer Control Protocol " rides" at the transport layer. Higher layers govern translating data or energy into a form appropriate for the application and hosting applications.

Many techniques developed for communication work well for transmitting energy in space or through the atmosphere. Extending the techniques of Ref 1, we will show how different approaches to orbit determination, different schemes for estimating orbits, and different approaches to assessing the probability of potentially damaging encounters affects firing windows.

Several methods are implemented for assessing the instantaneous risk of direct laser impingement given uncertainties in object and emitter positions. These methods determine when the probability of laser impingement exceeds a user-defined threshold. The probability of damage is the susceptibility of the unintentional target multliplied by the probability of impingement.

---

[*] Salvatore Alfano, Technical Program Manager, Center for Space Standards and Innovation
[†] Christopher T Kucera, Aerospace Systems Engineer, Analytical Graphics, Inc.
[‡] David Finkleman, Senior Scientist, Center for Space Standards and Innovation
7150 Campus Drive, Suite 260, Colorado Springs, Colorado, 80920

These approaches are new to the directed energy community and open a portal to a universe of protocol layer strategies developed for fixed and wireless communications.

Introduction

The terminology of the communications world is esoteric and unfamiliar to most.   It is logical, and the manner in which it parses the world is a good paradigm. The five lowest Open System Interconnect (OSI) layers are as follows.

- **PHYSICAL LAYER** *(THE ENVIRONMENT)*
    - **THE ENVIRONMENT MUST BE ABLE TO SUPPORT COMMUNICATIONS**
        - **CHANNEL LOSS (OBSTRUCTIONS, ATMOSPHERICS)**
        - **INTERFERENCE**
        - **MECHANICAL AND PHYSICAL INCOMPATIBILITIES**
- **DATA LINK LAYER** *(THE ROAD MAP)*
    - **MUST ESTABLISH PATHWAYS WITHIN THE COMMUNICATIONS MEDIUM AND MAKE PHYSICAL LINKS CONSISTENT (MAC)**
- **NETWORK LAYER** *(THE ROUTE)*
    - **MUST ACCOMMODATE CHANGES IN TOPOLOGY AND DISCOVER ROUTES (IP)**
- **TRANSPORT LAYER** *(THE TRAVELER FOLLOWING THE ROUTE)*
    - **MUST MATCH DELAY AND DROPOUT CHARACTERISTICS TO SUSTAIN RELIABLE (ERROR FREE) COMMUNICATION (TCP)**
- **APPLICATION LAYER**
    - **MUST BE ABLE TO HANDLE FREQUENT AND UNANTICIPATED DISCONNECTIONS (HLA)**

    -

Characteristics of the atmosphere and the interface with the atmosphere are the physical layer for directed energy applications. The protocols include beam transfer physical interfaces. Laser clearinghouse activities are at the link layer. The protocols are firing window characteristics. The network layer includes laser firing doctrines, and the transport layer governs actual transmission of the laser beam.

The communications community has a rich foundation of transmission schemes that could apply directly to transmitting laser energy to designated recipients (or targets). The "link margin" physical layer formalism is equivalent to the refractive, diffractive, scattering, and target coupling aspects of delivering laser energy.   The background distribution of satellites that must be considered is the link layer, determining the dynamic topology of objects in the "network." Determining actual firing windows to accomplish goals with quantified risk and probability of success is the network layer, the major aspect of this paper. Interaction with and feedback from the target is in the transport layer, within which the transmission is adjusted or modulated to match target availability and state.

Interrogating potential high energy beam paths with low power, auxiliary lasers is one example of a transport layer schema, similar to what Transfer Control Protocol (TCP) does for the Internet.   Electro-Optic Systems, Pty., employs such a system for the Australian element of the world-wide Satellite Laser Ranging (SLR) network. The approach has been approved for laser operations through controlled airspace by the Australian equivalent of the U.S. Federal Aviation Administration.

We are certain that many wireless communication OSI layer schemas are directly applicable to transmitting laser energy through the atmosphere and space with risk and success to suit the circumstance.

Most outside of the astrodynamics and aerial navigation community assume that the position and orientation of airborne platforms and satellites are known precisely. This is not so. Satellite position and velocity are uncertain to a degree that depends on the quality and distribution of observations, whether those observations are obtained remotely or onboard, cooperatively or uncooperatively. There are many different approaches to determining satellite orbits and estimating states of motion instantaneously and in the future. These add modeling uncertainties to measurement uncertainties. Rather than exercise judgment among the different orbit estimation techniques, algorithms used to determine laser firing windows accommodate uncertainty very conservatively, often denying firing opportunities that might be used effectively if uncertainties had been quantified reliably. The discussion that follows accommodates quantified uncertainty in our knowledge of where satellites will really be located.

Predictive avoidance analysis for laser emissions should reasonably ensure that neighboring objects are not inadvertently illuminated. Typically, one determines if and when a secondary object will transgress a user-defined circular safety cone[2,3]. The cone axis is along the line-of-sight vector as measured from the laser beam source to the primary object with its half-angle based on conservative estimates of positional accuracy (Fig 1). For space objects, prescreening of neighboring satellites can greatly reduce the computational burden[2]. For high-energy lasers, it is imperative to balance mission objectives against possible degradation or disruption of neighboring objects.
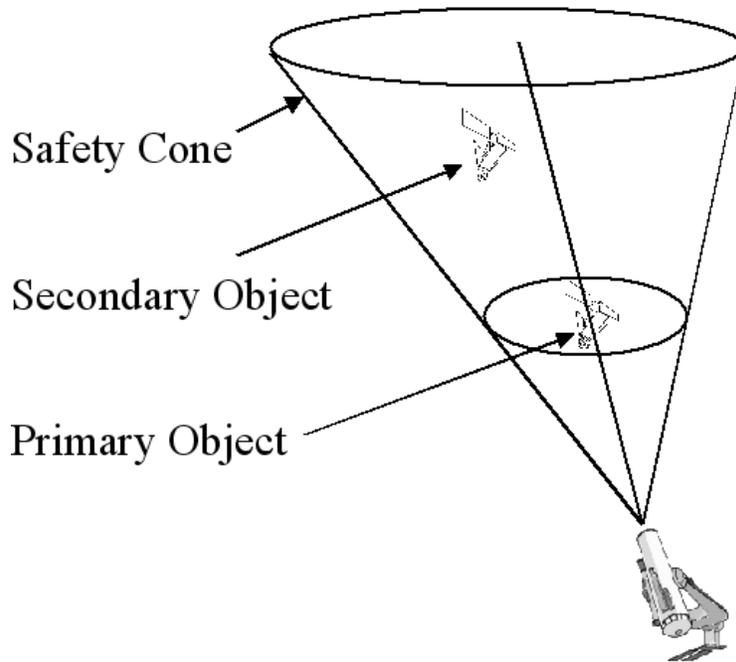
Fig. 1 Safety cone centered on primary object

　　If the uncertainties associated with emitter location and object position can be represented by three-dimensional Gaussian probability densities, then the true probability of direct laser impingement on a secondary object can be calculated directly. These densities take the form of covariance matrices and can be obtained from the owner-operators or independent surveillance sources such as the US Satellite Catalog (Special Perturbations). The traditional safety-cone approach is extremely conservative if the shape is not tailored to the probability density.. Such cones are circular and larger than necessary, scaled to the size of the axis of greatest uncertainty. As has been verified with launch collision avoidance, such conservatism can deny opportunities that have very low incidental probabilities[4]. Objects that are predicted to enter such cones should be further evaluated so as not to unnecessarily hinder operations.

　　The methods implemented here can be used to assess the instantaneous risk of direct laser impingement on a secondary object. Covariances of emitter and object locations are scaled, projected into a plane perpendicular to the beam, and then combined. Object and beam sizes, represented as circles in this encounter plane, are also combined and then translated to the mean location of the secondary in the plane. One determinant for window closure involves examining the scaled secondary and primary covariance ellipses to see if they touch. This approach does not require (or necessarily reveal) where they touch and is computationally very efficient and straightforward. A subsequent determinant for window closure could be the actual probability based on projected object sizes and covariances. A maximum probability assessment[10] can also be performed even if covariance information is unavailable.

All these methods can be combined to form cascading filters. As an example, one might first determine if the secondary object is inside the safety cone. If inside the cone, the primary and secondary covariances ellipses could then be examined to see if they touch. If they touch, then the maximum probability is computed. If the maximum probability exceeds a user's threshold, then the true probability is computed. Then the susceptibility of the satellite to illumination at the level anticipated can be convolved with the encounter probability to quantify actual risk. There can be many variations to implementation. It is not our intent to dictate which things must be done or in what specific order. It is our intent to provide an operator with sufficiently meaningful data to make an informed decision.

Preliminary Assessment

An initial assessment should be made to determine how average satellite visibility varies with azimuth and elevation for a given platform location and altitude. Hemispherical satellite population density maps can be created to identify areas that, in general, have a relatively low number of background objects. Such maps address average visibility and should not be considered as a substitute for a laser clearing algorithm that addresses specific, time-dependent, visibility.

It is extremely important that mean background density based estimates not be used for live laser illumination. These counterbalance high probability encounters with very low probability encounters, masking the real risk to satellites that might be at extreme risk. If is unfortunately very common for those who operate lasers to divide the number of satellites that might be at risk by the entire Earth orbiting population, most of which is not even line of sight to the illuminator.

By taking into consideration the average satellite background, laser engagements can be planned in such a way as to maximize firing opportunities while ensuring the safety of orbiting objects. Density maps provide a means to determine which portions of the sky are more likely to be open. Planners can use this information to formulate engagement geometries that consider launcher location, target trajectories, timing, and platform location and altitude, while also assessing which combinations minimize the general possibility of window closer.

A dome is created about the platform (Fig 2) and the azimuths and elevations of all satellites of interest are traced over time. A time average of satellites per azimuth/elevation grid is then computed and displayed as a polar plot. To circumvent distortion due to pinching of the grid near zenith, each grid average is computed per steradian.
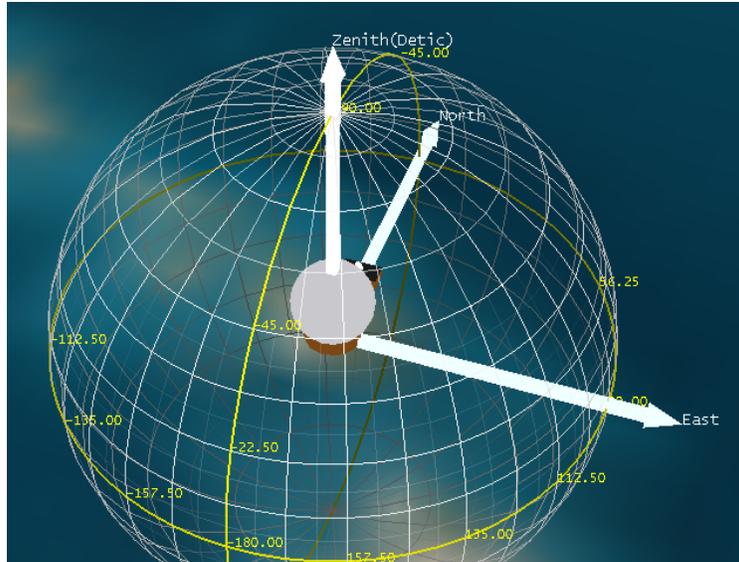
Fig. 2   Lasing Platform Hemispherical Dome

To perform this analysis, the Complete Method of Ratios[5] was used to determine average viewing periods of all satellites in a given catalog. The method computes average daily access time of a space object by a viewing platform with restrictions in azimuth, elevation, and range. The method makes extensive use of spherical trigonometry to rapidly arrive at viewing solutions. Because this is an averaging method, only site latitude is considered. Longitude is not needed because the method assumes that, over a long period of time, a space object is equally visible to all sites on a given latitude band.

Hemispherical satellite population density maps are created by simply subdividing the dome into grids of acceptable resolution, obtaining the average viewing periods of all satellites for each grid per steradian, summing, and displaying as a polar plot as seen in the following figures. North is at the top and South at the bottom. The center of the plot corresponds to what would be seen directly overhead (zenith) and the circumference shows what would be seen on the horizon. The shading goes from dark (low satellite density) to bright (high satellite density). The GEO belt and other satellites of low inclination can be clearly seen in the bright band that sweeps from east to west across the southerly region.
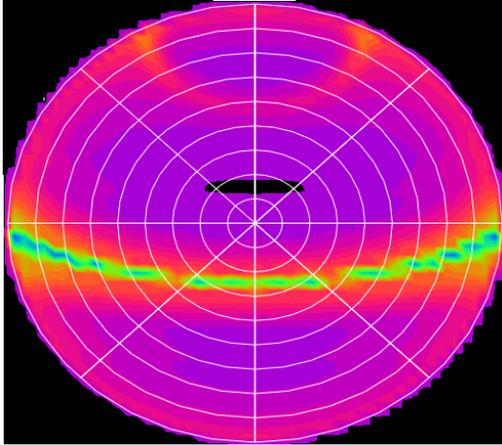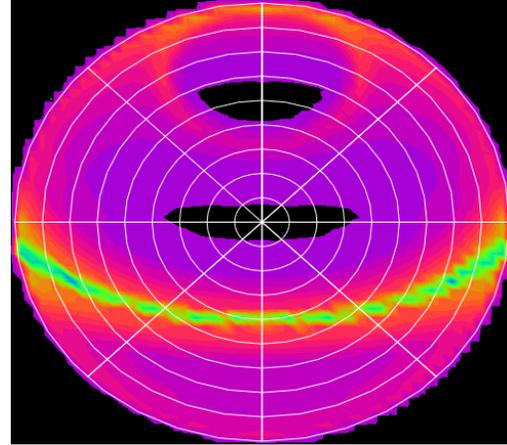
Fig. 3   AMOS Sat Density Map   **Fig. 4   SOR Sat Density Map**

The entire unclassified, publicly available, satellite catalog for September 16, 2005 (8,642 objects, including debris) was processed in combination with the Air Force Maui Optical Sight (AMOS) and Starfire Optical Range (SOR) to produce Figures 3 and 4. Similar maps can be made that contain a subset of the satellite catalog such as active payloads (functional satellites) or that exclude a subset such as the GEO belt.

Determining Projected Covariance Ellipse Overlap

Although two ellipsoids may not share the same space, when viewed from certain angles one may appear to cover or overlap the other (Fig 5). Analysis of such circumstances is necessary to prevent accidental laser illumination if a secondary object is in or near the line of sight of the primary. Line-of-sight projection is detailed in Ref 1 where covariances of emitter and object locations are scaled, projected onto a plane perpendicular to the beam, and then combined. Object and beam sizes, represented as circles in this encounter plane, are also projected and combined to produce Figure 6.
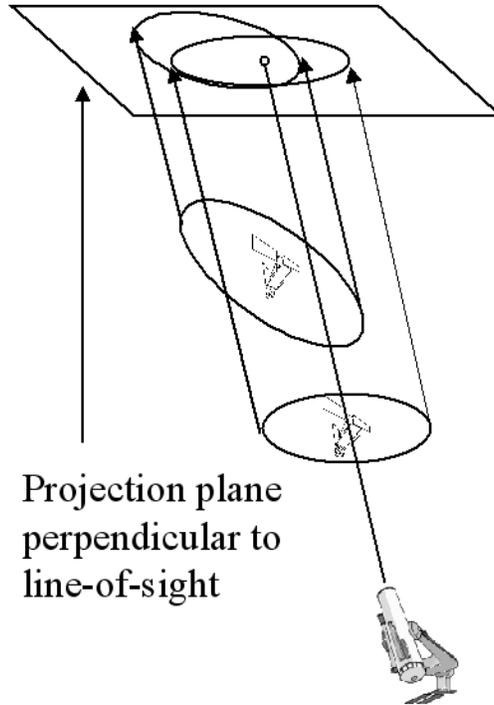
Fig. 5   Object and covariance projections on to the Encounter Plane
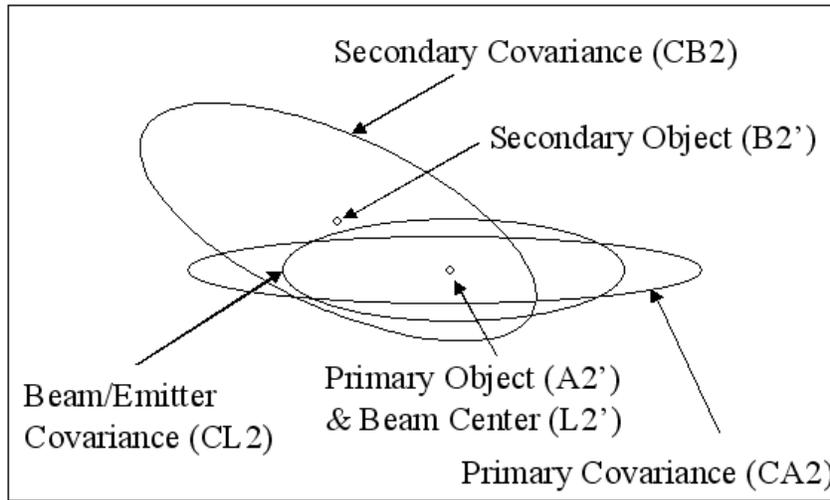

Fig. 6   Projections onto the Encounter Plane

The covariance matrices are assumed uncorrelated. After projection onto the encounter plane, the Beam/Emitter and Primary covariances can be summed to form a new ellipse in the plane. This ellipse and the Secondary covariance ellipse can then be scaled and examined to determine if they touch. The scale factor applied to the standard deviation should typically be in the range of 3 to 8, thereby accommodating impingement possibilities ranging from 97.070911% to 99.999999%.

An analytical method[6,7] to determine if ellipses overlap can be used to determine window closure. The method involves adding an extra dimension to the solution space and examining eigenvalues that are associated with degenerate quadric surfaces. As viewed from the laser emitter, this method creates elliptically shaped cones centered on the Primary and Secondary objects and then determines if those cones touch.

Probability and Its Estimate

The projection detailed in Figure 6 can also be used to compute the instantaneous probability of laser impingement[1]. The projected, two-dimensional covariances of the beam, primary, and secondary are summed to form C2. The projected radii of the beam, primary, and secondary are summed to form OBJ. The B2 vector represents the projected relative distance between the two objects as shown in the next figure.
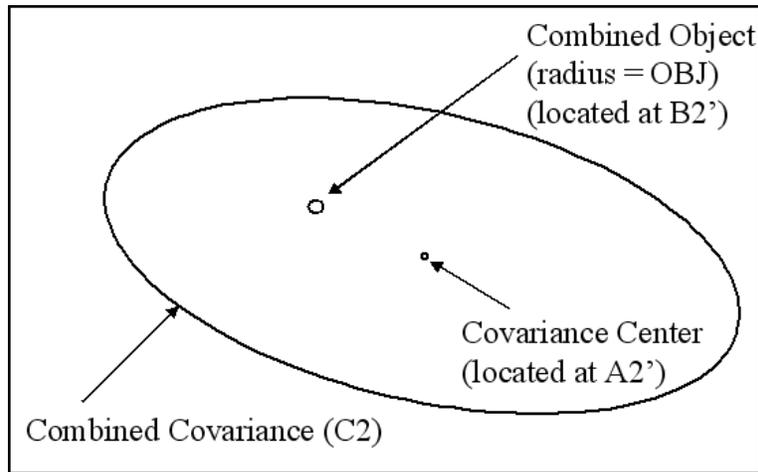

Fig. 7   Combined projection in the plane

With these definitions, the instantaneous probability P of laser impingement is computed from

$$P = \frac{\int_{B2_0-OBJ}^{B2_0+OBJ} \int_{B2_1-\sqrt{OBJ^2-(x-B2_0)^2}}^{B2_1+\sqrt{OBJ^2-(x-B2_0)^2}} \exp\left[\frac{-1}{2}\cdot\left[(x\ \ y)\cdot C2^{-1}\cdot\binom{x}{y}\right]\right] dy\ dx}{2\cdot\pi\cdot\sqrt{C2_{0,0}C2_{1,1}-(C2_{0,1})^2}} \cdot$$

The above equation can be reduced to a single integral using error functions, but its computation can still be burdensome. An alternate form of reduction can be found in Patera's work[8]. Algebraic approximations might also be appropriate for many cases[1,9].

Maximum Probability and Probability Dilution

For fixed object sizes and miss distance, the combined-covariance, minor axis, standard deviation (σx) that produces the maximum probability (Pmax) defines the dilution region boundary as shown in Figure 8. To the left of the vertical line, greater positional accuracy (smaller σx) decreases collision probability. To the right of the vertical line, lesser positional accuracy (greater σx) also decreases collision probability. Both good and poor quality data can produce the same probability (10^{-6} is given as an example in Fig 8). Although both calculations are mathematically correct, only the former is operationally meaningful to open or close a lasing window.
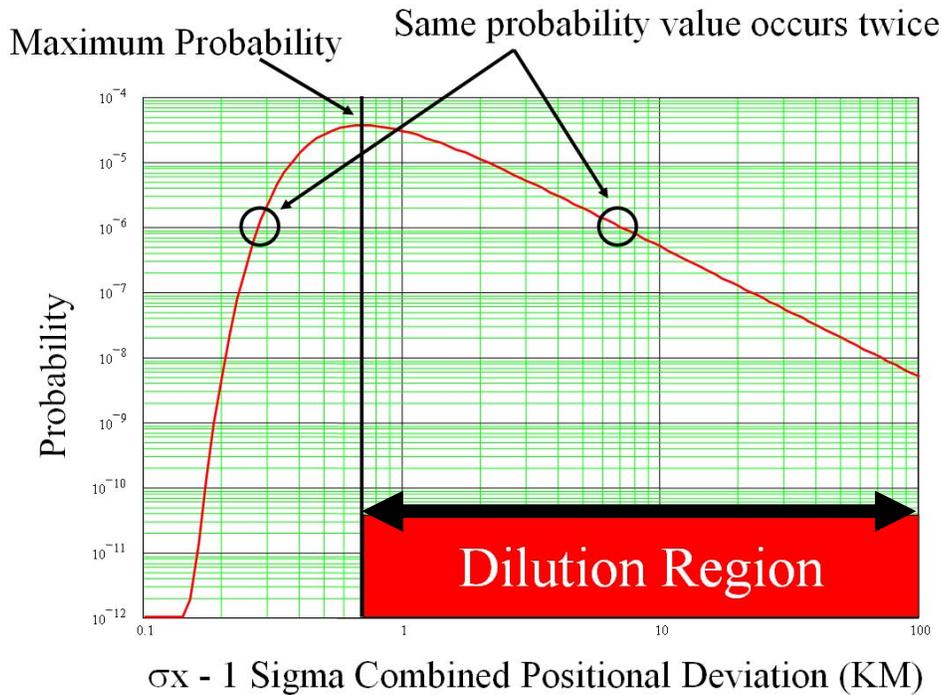

Fig. 8 Dilution Region Defined for Notional Encounter

The probability dilution region is that region where the standard deviation of the combined covariance minor axis (σx) exceeds that which yields Pmax. When operating outside this dilution region (left of vertical line), it is reasonable to associate low probability with low risk. Inside the dilution region, the further the uncertainty progresses the more unreasonable it becomes to associate low

probability with low risk. If the positional uncertainty is large enough, the resulting low probability misleads the user into thinking the encounter poses little or no threat. Therefore, a low probability in the dilution region may be the result of poor quality data and should be treated accordingly.

The dilution region boundary should be used to determine the minimum accuracy requirement for a meaningful probability assessment. When calculating true probability from equation (1), the reader is advised to always consider this region. If the positional data is not of sufficient quality to avoid this region, then get better (more accurate) data and reassess the true probability. If better data is not available or still insufficient, consider using the maximum probability[10] as opposed to the true one. This will ensure that a decision maker is not lulled into a false sense of security by a low probability calculation that is specious. Recognize however that the true probability might be orders of magnitude smaller than the maximum.

The maximum probability equation[11] is expressed as

$$P_{max} = \frac{1}{2 \cdot \pi \cdot AR \cdot \sigma x^2} \cdot \int_{-OBJ}^{OBJ} \int_{-\sqrt{OBJ^2-x^2}}^{\sqrt{OBJ^2-x^2}} \exp\left[\frac{-1}{2} \cdot \left[\left(\frac{x}{\sigma x} \right)^2 + \left(\frac{y + |B2|}{AR \cdot \sigma x} \right)^2 \right] \right] dy\, dx$$

where the aspect ratio (AR) is the ratio of the major-to-minor axes standard deviations. To determine the value of σx that maximizes the probability, the derivative of the above equation is taken with respect to σx and set to zero. An exact analytical solution does not exist, so a numerical search must be performed or an approximate expression used.

Choosing an Aspect Ratio

If the combined covariance is known, then AR is easily computed. If the combined covariance is unknown, the user must decide what aspect ratio is reasonable for analysis. If all orientations are assumed equally likely, then the aspect ratio will be one. For the absolute worst case imaginable the aspect ratio should be set to infinity which reduces Equation (2) to

$$P_{max} = \frac{1}{2} \cdot \left[erf\left[\frac{(r+1)}{2 \cdot \sqrt{r}} \cdot \sqrt{-\ln\left[\frac{(1-r)}{(1+r)} \right]} \right] + erf\left[\frac{(r-1)}{2 \cdot \sqrt{r}} \cdot \sqrt{-\ln\left[\frac{(1-r)}{(1+r)} \right]} \right] \right]$$

where

$$r = \frac{OBJ}{|B2|}$$

•

and the value of the standard deviation (σ_u) that maximizes the probability and defines the probability threshold is

$$\sigma_u = \sqrt{\frac{2 \cdot r}{\ln\left[\frac{(1 + r)}{(1 - r)}\right]}}.$$

•

It is instructional to get a sense of the aspect ratio's variability. Every day that new NORAD two-line element sets (TLEs) are publicly released, a maximum conjunction probability report is generated and posted as a free advisory service[12] at the website http://celestrak.com/SOCRATES/. The June 29, 2004, data was used to determine all object pairings of primaries (2,627) with secondaries (8,411) within 10 kilometers for a seven day span. This data was coupled with synthetic time-varying covariances produced by The Aerospace Corporation's COVGEN tool[13] . The combined aspect ratio for each of the resulting 26,752 pairs was then used to produce figures that show variability.

The reader is advised that the covariances used to produce the figures are not statistically formal due to the nature of COVGEN processing. The estimates of error and error growth for each object are obtained by processing a time history of SGP4 element sets for each object while assuming zero bias. The differences in the Radial, Transverse, and Normal components are then found and quadratic estimation models their error growth. This method can underestimate the initial error at epoch, so a separate method is used to determine such. If one is willing to consider COVGEN results as sufficiently proper representations of the TLE positional covariances then the following charts can be used to choose an acceptable bound for the aspect ratio.
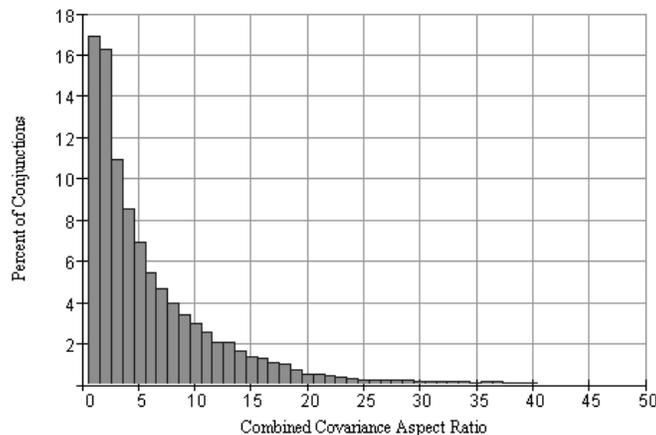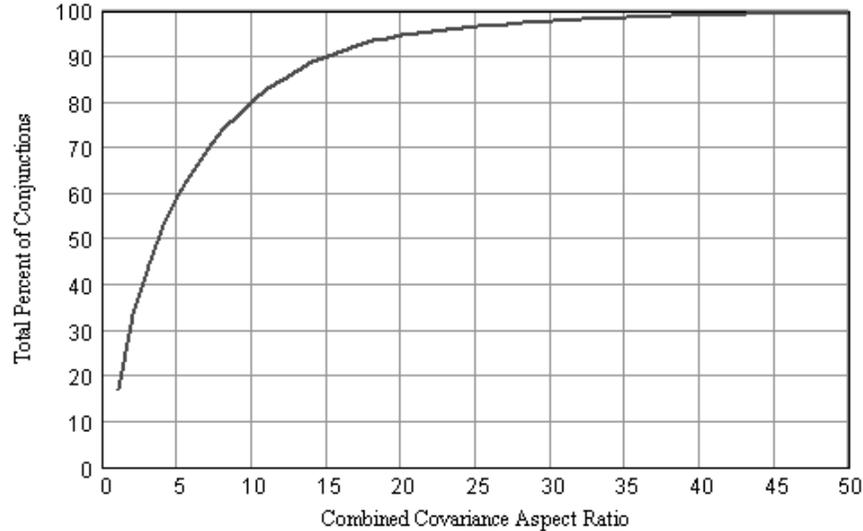

Fig. 9 Aspect Ratio Histogram

Fig. 10 Cumulative Percentage versus Aspect Ratio

The figures are representative of day-to-day occurrences. As seen in Fig 10, 99% of all conjunctions have an aspect ratio of 40 or less. 99.9% of all conjunctions have an aspect ratio of 70 or less (not shown). The maximum aspect ratio rarely exceeds 140.

It is obviously desirable to use the most representative covariances possible, thus ensuring the correct aspect ratio for each and every conjunction. A larger aspect ratio will result in a larger value for Pmax. Using a default aspect ratio of 40 or 70, sufficient to capture most conjunctions, will cause the maximum probability to be over-inflated for many of those conjunctions. Although not ideal, this may be the best assessment possible if the covariance data is insufficient or not available.

Implementation

Satellite Tool Kit (STK) was chosen to implement the probability portion of this Laser Clearinghouse algorithm because it already features the geometric analysis of safety cones (LaserCAT module) with terrain masking included. It also features a programming interface for user-built scripts to create a custom Graphical User Interface (GUI). Figure 11 shows the GUI for this particular implementation.

Fig. 11 Graphical User Interface

This application was written VBScript. An object is created to serve as the laser emitter (vertex of the safety cone). This object can be a ground-based

facility (static) or airborne (dynamic). The field of view for the cone is modeled as a sensor object and pointed either statically in azimuth and elevation or dynamically by tracking the target object in the scenario. Lasing window closures are initially assessed by determining when a secondary object from the NORAD space object catalog transgresses the moving safety cone.

The visibility constraints in STK make the problem more realistic and the results more accurate. For example, if lasing is to be performed only when the site is in the dark, the user can implement a sun constraint of "Umbra" ensuring that the night constraint is included. In our example, terrain constraints were used to calculate visibility with natural obstructions. Terrain data from the Shuttle Radar Topography Mission was added to the scenario to produce the following figure for the Starfire Optical Range (SOR).
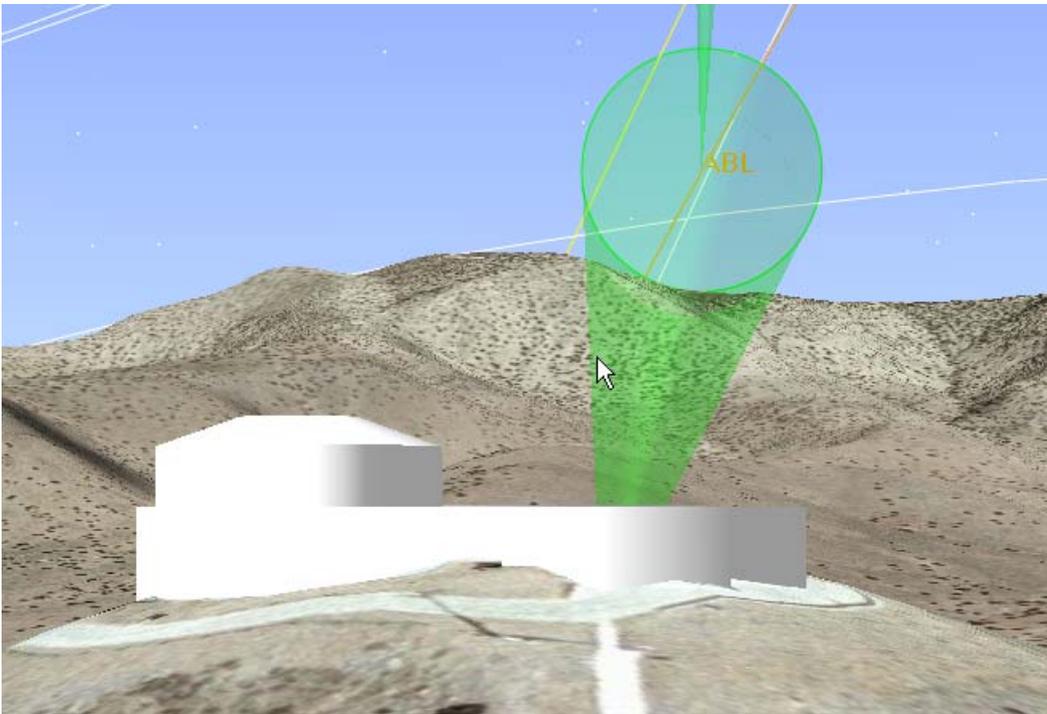

Fig. 12 Laser Safety Cone with Terrain Obstructions

The initial filter requires some basic inputs that are sufficient to capture all uncertainties in the problem. For our example
- The half cone angle was set to 2.5 degrees
- The cone shape was conical
- NORAD TLEs (with SGP4 propagation) were considered adequate
- Combined satellite covariance Aspect Ratio was set to one (AR=1) for the maximum probability calculation.

These can be easily modified or appended.

Upon completion of geometric filtering, STK returns a list of possible encounters. The script then cycles each encounter through a probability algorithm. For this example, position data was limited to the publicly available TLEs distributed by NORAD. The TLEs do not contain information about positional uncertainty. In the absence of covariance information, the maximum probability algorithm is implemented. If covariance is available, true probability can be implemented and Special Perturbation propagators used to obtain more accurate propagation results.

For each returned object in the initial cone filter, the script computes a step size between probability calculations by dividing the duration of the physical pass by twenty. The number is arbitrary, chosen here as sufficiently adequate for graphing probability results. At each step, the script queries STK for the position of the laser emitter, the target, and the secondary object. Object sizes for the target and secondary object are obtained by table lookup. The table contains the height, width, and length of each object and the root-sum-square defines object diameter. If the object is not found in the table, the object radius is set to three meters as suggested by Peterson[14].

Beam divergence is also required in the algorithm, chosen for this script as 0.00003 radians, which conservatively characterizes a many times diffraction limited 3 micron beam and a one meter aperture. The resulting probability is then sent to the Microsoft charting component to create a graph (Fig 13) over the cone encounter time.
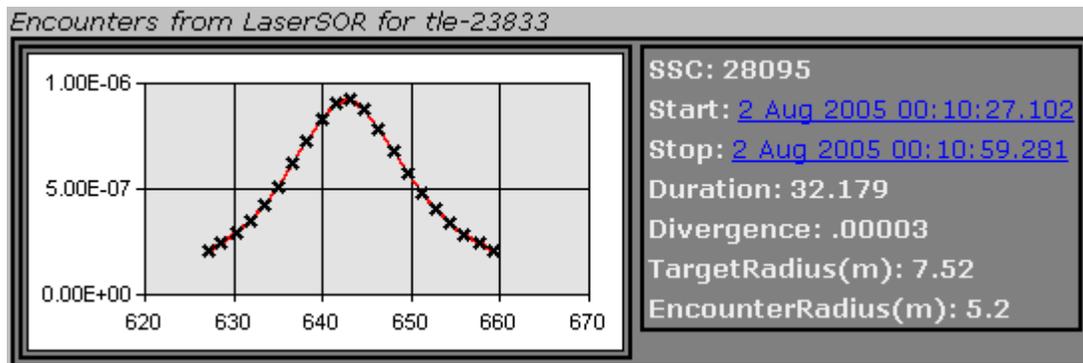

Encounters from LaserSOR for tle-23833

SSC: 28095
Start: 2 Aug 2005 00:10:27.102
Stop: 2 Aug 2005 00:10:59.281
Duration: 32.179
Divergence: .00003
TargetRadius(m): 7.52
EncounterRadius(m): 5.2

Fig. 13 Maximum Probability of Impingement within Laser Safety Cone as a Function of Time

This scenario was created for the SOR laser using a 2.5 degree half cone angle targeting satellite 23833 (NAVSTAR 37). The initial filter predicted that satellite 28095 (USA 173) would be in the safety cone for 32.2 seconds. If the impingement threshold was chosen to be one-in-a-million, then the entire 32.2 seconds would be available for lasing because the maximum probability never gets that high. If the impingement threshold was chosen to be five-in-ten-million, then laser operations would be required to cease for about 16 seconds. This

probability approach can restore opportunities that are denied with a safety cone-only approach.

Effects of Assumptions and Other Observations

Analysis is only as good as the assumptions on which it is based. Greater uncertainty in laser emitter location and/or satellite position can cause a dilution of the probability estimate. For such cases it might be prudent to examine the location that yields the greatest probability (i.e. worst case scenario) or use the maximum probability. One might assume that the primary object location is perfectly known if it is being illuminated; in that case its covaraince should be set to zero. No consideration was given in this work to the screening (shadowing) effect that the primary object might have on the secondary. The methods here can be easily altered to accommodate such occurrences. Models for diffraction, jitter, wavefront error, focus, aperture shape (rectangular versus circular), mode, and intensity pattern can be included to better define the beam size and its covariance.

This work examines the instantaneous risk of laser impingement whereas some satellites might be more vulnerable to the cumulative effects. Those satellites would require a different analysis, such as the one presented by Patera[8].

The methods implemented deal with laser impingement without consideration of the secondary satellite's tolerance to such. We have described how a satellites actual vulnerability can also be determined. An additional screening could be done to determine if a given satellite's known or stated threshold would be exceeded. Such a determination could eliminate a lot of space debris from the analysis.

This is one of a spectrum of schemas that are analogous to OSI layer communication procedures. This example can be expanded to multiple sequential laser firings and encounter optimization.

Conclusions

A software tool was built and demonstrated for assessing the instantaneous risk of direct laser impingement given uncertainties in object and emitter positions. The primary and secondary objects are modeled as spheres and projected to a plane perpendicular to the laser boresight; beam width (divergence) was also included. Covariances of the objects and emitter location are combined and also projected onto the plane after appropriate scaling. The probability of laser impingement is determined from the relation of combined object area to combined covariance. In the absence of covariance information, maximum probability is computed.

REFERENCES

1. Alfano, S., "Assessing the Instantaneous Risk of Direct Laser Impingement," *AIAA Journal of Spacecraft and Rockets*, Vol. 40, No. 5, September-October 2003, pp. 678-681.
2. Alfano, S., Burns, R., Pohlen, D., and Wirsig, G., "Predictive Avoidance for Ground-Based Laser Illumination," *AIAA Journal of Spacecraft and Rockets*, Volume 37, Number 1, pp. 122-128.
3. Morris, R. F., and Racca, R. A., "Theater High Energy Laser (THEL) SkyPlot Software Validation," Space Warfare Center Analysis & Engineering Technical Report 99-12, November 1999.
4. Oltrogge, D., and Gist, R., "Collision Vision Situational Awareness for Safe and Reliable Space Operations," 50th International Astronautical Congress, 4-8 Oct 1999/Amsterdam, The Netherlands, IAA-99-IAA.6.6.07
5. Alfano, S., and Negron D., "Complete Method of Ratios," *AIAA Journal of Spacecraft and Rockets*, Volume 30, Number 3, May-June 1993, pp. 374-379.
6. Chan, K., "A Simple Mathematical Approach for Determining Intersection of Quadratic Surfaces," AAS/AIAA Astrodynamics Specialist Conference, July 30 – August 2, 2001, Quebec City, Canada, AAS 01-358.
7. Alfano, S., and Greer, M. L., "Determining if Two Ellipsoids Share the Same Volume," AAS/AIAA Astrodynamics Specialist Conference, July 30 – August 2, 2001, Quebec City, Canada, AAS 01-357.
8. Patera, R. P., "The Probability of a Laser Illuminating a Space Object," *AIAA Journal of Spacecraft and Rockets*, Volume 40, Number 1, January-February 2003, pp. 114-118.
9. Chan, K., "Improved Analytical Expressions for Computing Spacecraft Collision Probabilities," AAS/AIAA Space Flight Mechanics Meeting, February 9-13, 2003, Ponce, Puerto Rico, AAS 03-184.
10. Alfano, S., "Relating Position Uncertainty to Maximum Conjunction Probability," AAS/AIAA Astrodynamics Specialist Conference, August 3-7, 2003, Big Sky Resort, Big Sky, Montana, AAS 03-548.
11. Alfano, S., "Collision Avoidance Maneuver Planning Tool," AAS/AIAA Astrodynamics Specialist Conference, August 7-11, 2005, Lake Tahoe, California, AAS 05-308.
12. Kelso, T.S., and Alfano, S. "Satellite Orbital Conjunction Reports Assessing Threatening Encounters in Space (SOCRATES)," AAS Paper No. 05-124, AAS/AIAA Space Flight Mechanics Meeting, 23-27 January, 2005, Copper Mountain, Colorado.
13. Peterson, G. E., Gist, R. G., and Oltrogge, D. L., "Covariance Generation for Space Objects using Public Data," AAS Paper No. 01-113, AAS/AIAA Space Flight Mechanics Meeting, 11-15 February, 2001, Santa Barbara, California.
14. Peterson, G. E., "Determining Object Sizes form Radar Cross Sections for Collision Avoidance," AAS Paper No. 05-307, Astrodynamics Specialist Conference, 7-11 August, 2005, Lake Tahoe, California.